Constant-energetics physical-space forcing methods for improved convergence to homogeneous-isotropic turbulence with application to particle-laden flows

Maxime Bassenne, Javier Urzay, George I. Park, and Parviz Moin

Citation: Physics of Fluids **28**, 035114 (2016); doi: 10.1063/1.4944629
View online: http://dx.doi.org/10.1063/1.4944629
View Table of Contents: http://scitation.aip.org/content/aip/journal/pof2/28/3?ver=pdfcov
Published by the AIP Publishing

PHYSICS OF FLUIDS **28**, 035114 (2016)

Constant-energetics physical-space forcing methods for improved convergence to homogeneous-isotropic turbulence with application to particle-laden flows

Maxime Bassenne, Javier Urzay,[a] George I. Park, and Parviz Moin
Center for Turbulence Research, Stanford University, Stanford, California 94305-3024, USA

(Received 5 October 2015; accepted 9 March 2016; published online 30 March 2016)

This study investigates control-based forcing methods for incompressible homogeneous-isotropic turbulence forced linearly in physical space which result in constant turbulent kinetic energy, constant turbulent dissipation (also constant enstrophy), or a combination of the two based on a least-squares error minimization. The methods consist of proportional controllers embedded in the forcing coefficients. During the transient, the controllers adjust the forcing coefficients such that the controlled quantity achieves very early a minimal relative error with respect to its target stationary value. Comparisons of these forcing methods are made with the non-controlled approaches of Rosales and Meneveau ["Linear forcing in numerical simulations of isotropic turbulence: Physical space implementations and convergence properties," Phys. Fluids **17**, 095106 (2005)] and Carroll and Blanquart ["A proposed modification to Lundgren's physical space velocity forcing method for isotropic turbulence," Phys. Fluids **25**, 105114 (2013)], using direct numerical simulations (DNS) and large-eddy simulations (LES). The results indicate that the proposed constant-energetics forcing methods shorten the transient period from a user-defined artificial flow field to Navier-Stokes turbulence while maintaining steadier statistics. Additionally, the proposed method of constant kinetic-energy forcing behaves more robustly in coarse LES when initial conditions are employed that favor the occurrence of subgrid-scale backscatter, whereas the other approaches fail to provide physical turbulent flow fields. For illustration, the proposed forcing methods are applied to dilute particle-laden homogeneous-isotropic turbulent flows; the results serve to highlight the influences of the forcing strategies on the disperse-phase statistics. [http://dx.doi.org/10.1063/1.4944629]

I. INTRODUCTION

Numerical simulation of homogeneous-isotropic turbulence in statistically stationary conditions requires forcing the Navier-Stokes equations in order to avoid the necessary decay caused by the dissipation of energy. In incompressible flows, one way of forcing consists of adding a linear term to the momentum equation,[1]

$$\frac{\partial u_i}{\partial t} + u_j \frac{\partial u_i}{\partial x_j} = -\frac{1}{\rho}\frac{\partial p}{\partial x_i} + \nu \frac{\partial^2 u_i}{\partial x_j \partial x_j} + A u_i, \tag{1}$$

where u_i are velocity components, p is the hydrodynamic pressure, ν is the kinematic viscosity, ρ is the density, and x_i denote spatial coordinates in a triply periodic domain. The forcing coefficient, A, is an unclosed quantity whose only modeling requirement is to enable and sustain statistically stationary homogeneous-isotropic turbulence. Equation (1) is to be solved along with the continuity equation

[a] Author to whom correspondence should be addressed. Electronic mail: jurzay@stanford.edu

$$\frac{\partial u_i}{\partial x_i} = 0. \tag{2}$$

Initial conditions used for integrating (1) and (2) typically involve a synthetic, solenoidal-isotropic velocity field with a prescribed energy spectrum. Such a field can be generated, for instance, by employing the kinetic-energy model spectrum[2]

$$E_0(\kappa) = \frac{32k_0}{3\kappa_0}\sqrt{\frac{2}{\pi}}\left(\frac{\kappa}{\kappa_0}\right)^4 \exp\left[-2\left(\frac{\kappa}{\kappa_0}\right)^2\right], \tag{3}$$

and by subsequently calculating the corresponding initial velocity components u_i from their Fourier transforms subject to random phases and a divergence-free condition. In this formulation, κ is the wavenumber, and κ_0 is the corresponding value at which the energy maximum $dE_0/d\kappa = 0$ is initially prescribed. In addition, $k_0 = \int_0^\infty E_0(\kappa)d\kappa$ is the initial turbulent kinetic energy. It should be emphasized, however, that the long-time solution of the problem (1) and (2) is independent of the parameters κ_0 and k_0.

As pointed out by Lundgren,[1] linear forcing has beneficial characteristics. For instance, linear forcing is congruent with the "2/3" Kolmogorov's law for the radial dependence of the second-order longitudinal structure function in the inertial subrange. However, linear forcing corresponds to injecting energy in all wavenumbers. This is in contrast to forcing approaches in spectral space, in which energy injection is limited to wavenumber bands.[3] Although band-limited forcing generally leads to different integral lengths, the differences between turbulent flows forced in spectral and physical spaces are small, partly because the energy injected by the physical-space forcing method at large wavenumbers is negligible compared with that injected at small wavenumbers (e.g., see Fig. 12 in Ref. 4). In practice, linear forcing in physical space, as in Eq. (1), is an attractive low-cost method for numerical codes that are not formulated spectrally. The challenge, however, lies in providing a suitable definition of the forcing coefficient A that enables fast convergence to statistically stationary homogeneous-isotropic turbulence.

Integration of Eqs. (1) and (2), subject to triply periodic boundary conditions and to the initial spectrum (3), provides a homogeneous-isotropic turbulent flow whose statistics should be steady after a transient period, during which the flow relaxes from the initial field to Navier-Stokes turbulence. After the transient, the flow is expected to attain long-time, steady mean values of the spatially averaged turbulent kinetic energy and turbulent dissipation that are denoted here by k_∞ and ϵ_∞, respectively. Besides the form of the forcing coefficient A, the dimensional input parameters to be specified are ρ, ν, and the computational domain side length L. That the solution depends on L can be understood from the linear forcing term in Eq. (1), which injects energy in amounts proportional to the energy content at each wavenumber, including that of the lowest non-zero wavenumber $\kappa_{min} = 2\pi/L$. The resulting integral length, $\ell_\infty = u_{\ell,\infty}^3/\epsilon_\infty$, with $u_{\ell,\infty} = (2k_\infty/3)^{1/2}$, the turnover velocity of the large-scales, oscillates with amplitude 20%-30% around the value $0.19L$ independent of all other input parameters (e.g., see Fig. 9 in Ref. 4).

The conservation equation for the turbulent kinetic energy, $k(t) = \langle u_i' u_i' \rangle/2$, is

$$\frac{dk}{dt} = -\epsilon + 2Ak, \tag{4}$$

where $\epsilon(t) = \langle \nu(\partial u_i'/\partial x_j)(\partial u_i'/\partial x_j)\rangle$ is the turbulent dissipation. In this formulation, the bracketed operator "$\langle f \rangle$" represents spatial averaging of f over the triply periodic domain, while the velocity perturbations u_i' are just taken to be the velocities u_i since the spatially averaged velocity $\langle u_i \rangle$ vanishes in this flow. As indicated by Eq. (4), the constant forcing coefficient

$$A = \epsilon_\infty/(2k_\infty) \tag{5}$$

is, in principle, required in order to sustain a turbulent flow with statistically stationary values of turbulent kinetic energy and turbulent dissipation, $k = k_\infty$ and $\epsilon = \epsilon_\infty$. Equation (5), which is equivalent to prescribing a constant integral time $t_{\ell,\infty} = \ell_\infty/u_{\ell,\infty} = 1/(3A)$, was used in numerical simulations by Rosales and Meneveau.[4]

The utilization of the constant forcing coefficient (5) is convenient for its simplicity. However, this approach has caveats. For instance, a long transient time of several integral times is typically

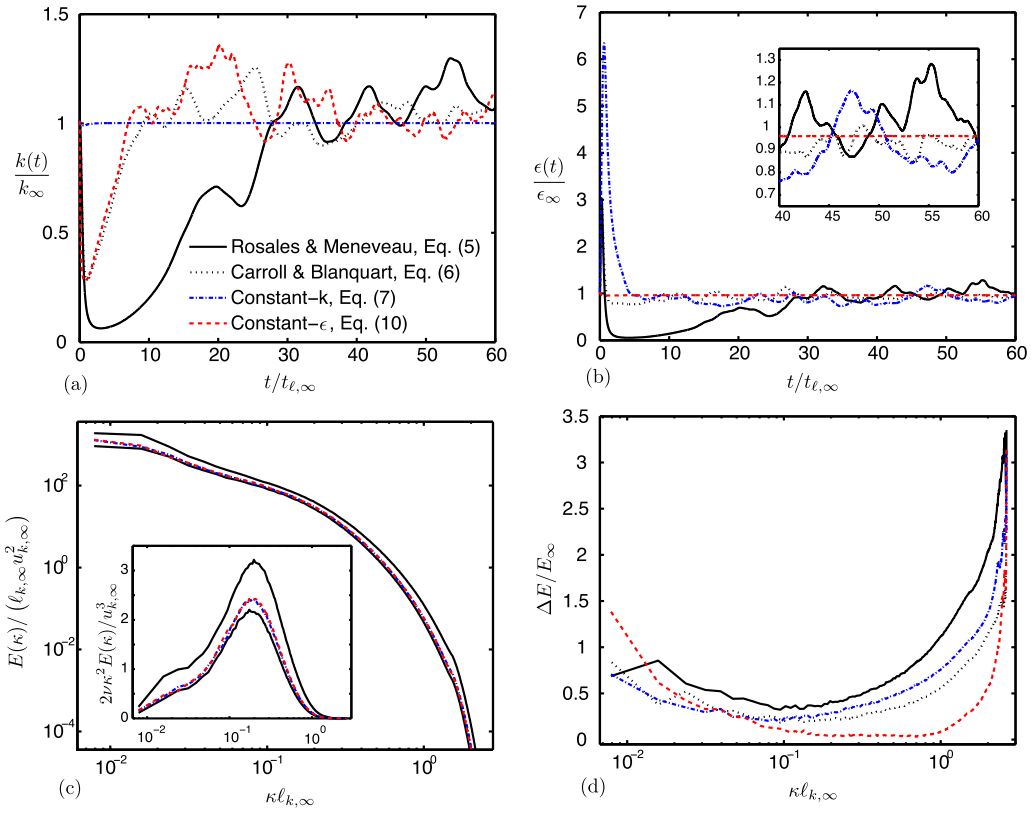

FIG. 1. DNS comparisons of the proposed forcing methods, with $G = H = 67$, against methods in Refs. 4 and 6 (see legend in panel (a) for line types). The upper panels include the time dependence of (a) turbulent kinetic energy and (b) turbulent dissipation. Panel (c) shows the instantaneous spectra of kinetic-energy and dissipation (inset), evaluated at $t = 5.7t_{\ell,\infty}$ (using (7)) and $t = 7.1t_{\ell,\infty}$ (using (10)), along with the envelope represented by the maximum and minimum values resulting from employing (5) during long periods of time $t = 43t_{\ell,\infty} - 72t_{\ell,\infty}$ (solid lines). Panel (d) shows the normalized amplitude of the envelopes produced by the maximum and minimum values of the kinetic-energy spectra observed during the time interval $t = 43t_{\ell,\infty} - 72t_{\ell,\infty}$ for all four methods.

required for the flow to become independent of the initial spectrum (3) and achieve acceptable values of the turbulent kinetic energy around the steady value, k_∞. Additionally, after such a long transient, the resulting values of k and ϵ oscillate in relative amounts of order 30%-40%, which in practice prevents the turbulent flow from reaching a statistically steady state, in that the spatially averaged statistics depend heavily on time (e.g., see Figs. 1 and 5-7 in Ref. 4 and Figs. 1(a) and 1(b) above). Note that increasing the spatial sampling size by increasing the computational domain length L at constant Reynolds number does not palliate the oscillations since the ratio ℓ_∞/L remains approximately constant in physical-space forcing. As discussed previously, this represents an intrinsic limitation of the approach for reaching stationarity. As a result, the turbulent flow resulting from integration of Eqs. (1) and (2) subject to (3) and (5) is typically far from statistically stationary conditions and is spatially homogeneous and isotropic only in the ensemble mean or time average. Similar oscillations in k and ϵ also arise in turbulent flows forced in spectral space. Relaxation approaches have been envisioned that overcome this problem in spectral-space forcing[3] and physical-space anisotropic forcing.[5] It is worth mentioning that the forcing methods proposed here are formally different than those addressed recently in Ref. 5, but have not been extended to anisotropic flows.

In a recent paper, Carroll and Blanquart[6] partly addressed the disadvantages outlined above by using a penalization of the forcing coefficient based on the instantaneous turbulent kinetic energy,

$$A(t) = \left(\frac{\epsilon_\infty}{2k_\infty}\right)\left[\frac{k_\infty}{k(t)}\right], \tag{6}$$

in such a way that forcing is deterred during upsurges of kinetic energy and vice-versa. An advantage of the time-dependent forcing coefficient (6) is that the observed oscillation amplitudes of k and ϵ decrease to 20%-30% with respect to the target values k_∞ and ϵ_∞, while the transient period becomes shorter (e.g., see Figs. 1 and 2 in Ref. 6 and Figs. 1(a) and 1(b) above). Note that an expression similar to Eq. (6) had been previously used for band-limited spectral forcing (see Eq. (4) in Ref. 7). The forcing method (6) corresponds to constant production of kinetic energy.

The forcing methods (5) and (6) do not yield constant values of turbulent kinetic energy and turbulent dissipation except during a hypothetical steady state which is not necessarily reached according to the conservation equations resulting from using the corresponding forcing coefficients. This can be easily understood by substituting Eq. (5) or (6) into Eq. (4) and observing that those definitions of A do not impose any direct constraint on the time derivatives of k or ϵ. In this study, forcing approaches are investigated that provide a prescribed constant kinetic energy $k = k_\infty$, constant dissipation $\epsilon = \epsilon_\infty$, or a suitable combination of both, preventing upsurges or downturns of large-scale turbulence energetics in order to reduce the time window required to extract stationary statistics. In Section II, alternative, constant-energetics control-based forcing coefficients are provided that are extensions of the two methods outlined above. The proposed methods are illustrated for direct numerical simulation (DNS) in Section III, where it is shown that they lead to improved convergence to Navier-Stokes turbulence. Furthermore, DNS solutions extracted from the forced flows are used as initial conditions for decaying turbulence, an approach that yields differences in velocity-derivative skewness convergence with respect to computations initialized with synthetic fields. The large-eddy simulation (LES) formulations of the proposed forcing coefficients, described in Section IV, are shown to exhibit similar benefits as in DNS. Additionally, the proposed coefficient for constant kinetic-energy forcing behaves more robustly in coarse LES, in that it yields physical solutions when initial conditions favoring the occurrence of subgrid-scale backscatter are employed. On the other hand, the other strategies fail to provide forced LES turbulence in this scenario. Lastly, an application of the proposed methods to dilute particle-laden turbulent flows is presented in Section V, which addresses the influence of the choice of the forcing approach on the statistics of the disperse phase. Section VI contains concluding remarks and a formulation in spectral space of the constant kinetic-energy forcing coefficient.

II. DNS FORMULATION OF CONSTANT-ENERGETICS CONTROL-BASED FORCING COEFFICIENTS

In this section, expressions for the forcing coefficient A are provided which ensure constant turbulent kinetic energy or constant turbulent dissipation, the latter also corresponding to constant enstrophy in the incompressible limit. A third forcing method is presented in which a combination of approximate constant values of dissipation and kinetic energy is achieved by a least-squares minimization. The description is accompanied by the resulting conservation equations for the spatially-averaged energetics.

A. Forcing at constant turbulent kinetic energy

Imposition of constant kinetic-energy forcing is made by the use of the forcing coefficient

$$A(t) = \frac{\epsilon(t) - G[k(t) - k_\infty]/t_{\ell,\infty}}{2k(t)}, \tag{7}$$

where G is a dimensionless constant that plays the role of a proportional gain. In particular, substitution of the time-dependent forcing coefficient (7) into (4) leads to the equation

$$\frac{dk}{dt} = -\frac{G(k - k_\infty)}{t_{\ell,\infty}}, \tag{8}$$

which, for a constant value of G, indicates that the turbulent kinetic energy k approaches exponentially fast to the steady value k_∞ with a time constant $t_{\ell,\infty}/G$. Specifically, $k = k_\infty$ is a stable equilibrium being satisfied after times of order $t_{\ell,\infty}/G$. Exceptions are found at order-unity values of G, for which offset errors prevent convergence to the target steady value of the kinetic energy if

the dissipation is not discretized consistently with the conservation equations, as shown below. It is worth emphasizing that the forcing coefficients (5)–(7) are exactly equivalent in the statistically stationary conditions $k = k_\infty$ and $\epsilon = \epsilon_\infty$.

B. Forcing at constant turbulent dissipation (also constant enstrophy)

The philosophy employed in Eq. (7) for imposing constant kinetic energy in Eq. (4) could be similarly utilized in order to demand constant dissipation. To see this, consider the turbulent dissipation equation

$$\frac{d\epsilon}{dt} = -2\nu\left\langle \frac{\partial u_i'}{\partial x_k}\frac{\partial u_j'}{\partial x_k}\frac{\partial u_i'}{\partial x_j}\right\rangle - 2\nu^2\left\langle \frac{\partial}{\partial x_j}\left(\frac{\partial u_i'}{\partial x_k}\right)\frac{\partial}{\partial x_j}\left(\frac{\partial u_i'}{\partial x_k}\right)\right\rangle + 2A\epsilon, \tag{9}$$

which is readily obtained by differentiating (1) with respect to x_k, multiplying the resulting equation by $2\nu\partial u_i'/\partial x_k$, and performing the corresponding spatial averaging over the periodic domain. In particular, the forcing coefficient

$$A(t) = -\frac{w(t) + H[\epsilon(t) - \epsilon_\infty]/t_{\ell,\infty}}{2\epsilon(t)}, \tag{10}$$

with $w(t)$ being the sum of the first two terms on the right hand side of (9), transforms Eq. (9) into

$$\frac{d\epsilon}{dt} = -\frac{H(\epsilon - \epsilon_\infty)}{t_{\ell,\infty}} \tag{11}$$

and yields constant dissipation $\epsilon = \epsilon_\infty$ after time scales of order $t_{\ell,\infty}/H$, where H is a constant proportional gain. Similarly, offset errors may occur when order-unity values of H are employed, which prevent convergence to the target steady value of the dissipation. In practice, the gains G and H will be taken to be large numbers such that the forcing develops under effectively constant-k or constant-ϵ conditions.

For the incompressible flows addressed here, the constant-ϵ forcing described by Eq. (10) is equivalent to constant-Ω forcing, with Ω denoting the enstrophy. This can be easily understood by substituting (10) with $\epsilon = \epsilon_\infty$ in the corresponding enstrophy conservation equation, which leads to $d\Omega/dt = 0$, or by noticing that the dissipation and enstrophy spectra are multiples of each other, so that the area Ω under the enstrophy spectrum must remain constant if ϵ is constant.

C. Approximate combination of constant-energy and constant-dissipation forcing

Since imposing (7) and (10) simultaneously is not possible, a hybrid forcing coefficient can be sought in the form

$$\begin{aligned} A(t) = {} & \frac{4k^2(t)}{4k^2(t) + 9t_{\ell,\infty}^2\epsilon^2(t)}\left(\frac{\epsilon(t) - G[k(t) - k_\infty]/t_{\ell,\infty}}{2k(t)}\right) \\ & - \frac{9t_{\ell,\infty}^2\epsilon^2(t)}{4k^2(t) + 9t_{\ell,\infty}^2\epsilon^2(t)}\left(\frac{w(t) + H[\epsilon(t) - \epsilon_\infty]/t_{\ell,\infty}}{2\epsilon(t)}\right), \end{aligned} \tag{12}$$

which is obtained by a least-squares minimization of the errors of Eqs. (4) and (9) with respect to the steady state $dk/dt = 0$ and $d\epsilon/dt = 0$. As a consequence, utilization of the forcing coefficient (12) does not yield constant values of k and ϵ, but the resulting dynamics are always intermediate with respect to these two extrema.

III. DNS RESULTS AND COMPARISONS

DNS are employed here to compare turbulent flows forced with the proposed coefficients (7) and (10) against those forced with (5) and (6). All simulations start from the same initial spectrum (3) and are subject to the same input parameters ($L = 2\pi$, $\nu = 0.005$, $\rho = 1.2$, $k_\infty = k_0 = 17.1$, $\epsilon_\infty = 32.3$, and $\kappa_0 = 12.5$, all quantities being expressed in arbitrary yet consistent units). The

resulting Taylor-Reynolds number of the turbulence is $\mathrm{Re}_\lambda = (15u_{\ell,\infty}\ell_\infty/\nu)^{1/2} = 110$. The calculations are conducted on a staggered, uniform Cartesian grid of 384^3 points, which translates into a resolution $\kappa_{max}\ell_{k,\infty} = 1.5$, where κ_{max} is the largest wavenumber resolved by the grid and $\ell_{k,\infty} = (\nu^3/\epsilon_\infty)^{1/4} = u_{k,\infty}t_{k,\infty}$ is the Kolmogorov length, with $u_{k,\infty} = (\epsilon_\infty\ell_{k,\infty})^{1/3}$ and $t_{k,\infty} = \ell^2_{k,\infty}/\nu$ being the Kolmogorov velocity and time scale, respectively. The Navier-Stokes equations (1) and (2) are solved with a finite-difference energy-conserving discretization of second order central in space and fourth-order Runge-Kutta in time.[10,11]

A. Convergence in physical and spectral spaces

Comparisons are made in Fig. 1 between DNS performed using the forcing coefficients outlined above, showing that the proposed coefficients (7) and (10) generally lead to steadier statistics and faster convergence in comparison to the methods (5) and (6) from Refs. 4 and 6. In particular, after a short transient $0 < t \lesssim 1.0t_{\ell,\infty}$, during which the kinetic energy is not strictly constant, Eq. (7) leads to a flat profile of k while (5) and (6) cause a delayed convergence and an ever-oscillating time dependence, as shown in Fig. 1(a). Similar conclusions are obtained by using Eq. (10), in that the constant dissipation is established rapidly in Fig. 1(b) leading to oscillations in the turbulent kinetic energy which are nonetheless comparable to those obtained using (6) and much less accentuated than those arising from (5). Additionally, after short transients the proposed coefficients (7) and (10) yield physically meaningful values of higher-order statistics, such as the skewness of the velocity derivative (not shown here for brevity), thereby indicating that utilization of constant-energetics forcing enables prompt convergence to the target state of Navier-Stokes turbulence.

None of the three forcing approaches (5)–(7) have direct control over the turbulent dissipation. As a result, the time dynamics of the turbulent dissipation are similar for all three methods, with the longest transient for this variable being obtained using Eq. (5), as shown in Fig. 1(b). The short transient $0 < t \lesssim 6.0t_{\ell,\infty}$ for the dissipation obtained using Eq. (6) is nonetheless counteracted by the delayed convergence of the turbulent kinetic energy. Conversely, the constant-k forcing (7) results in an overall faster convergence of k and ϵ to values near their target ones after a transient $0 < t \lesssim 5t_{\ell,\infty}$, in contrast to the longer transients $0 < t \lesssim 30t_{\ell,\infty}$ (using Eq. (5)) and $0 < t \lesssim 10t_{\ell,\infty}$ (using Eq. (6)). Utilization of the constant-ϵ forcing (10) leads to flat profiles of ϵ but longer transients for the kinetic energy than those obtained for the dissipation using constant-k forcing.

The instantaneous kinetic-energy spectra obtained at short times using the proposed coefficients (7) and (10), evaluated at $t = 5.7t_{\ell,\infty}$ and $t = 7.1t_{\ell,\infty}$, respectively, lie within the envelope represented by the maximum and minimum values resulting from employing (5) during long periods of time $t = 43t_{\ell,\infty} - 72t_{\ell,\infty}$, as shown in Fig. 1(c). Similar observations are made with respect to the dissipation spectra. At each wavenumber, the envelopes are defined as the extrema of the spectral kinetic energy and dissipation collected during the time interval $43t_{\ell,\infty} < t < 72t_{\ell,\infty}$. In general, the spectral envelope resulting from utilization of Eq. (5) is the thickest one, an effect being related to the comparatively larger variations in k and ϵ observed in Figs. 1(a) and 1(b). The constant-k forcing shows a superior spectral performance, with exceptions found in the much-less-energetic viscous-dissipation range where (6) provides less variability, as shown in Fig. 1(d). Conversely, the constant-ϵ forcing yields minimal spectral variations at high wavenumbers, but it underperforms at large scales where the other methods display less fluctuations.

The utilization of the hybrid coefficient (12) leads to intermediate results with respect to those described above, as shown in the DNS results in Fig. 2 where the same input parameters have been used. Specifically, the resulting oscillations in ϵ and k are smaller than those obtained by using (7) or (10) separately, while the relatively short transient period to Navier-Stokes turbulence is preserved. Because of the intermediate character of the hybrid approach, no further tests of (12) will be provided in this study.

B. Selection of the proportional gains

The effects of the proportional gains G in Eq. (7) and H in Eq. (10) are illustrated in Fig. 3, which shows numerical results from the same DNS described above for four different values of these parameters. In particular, large values of G and H favor faster convergence. On the other

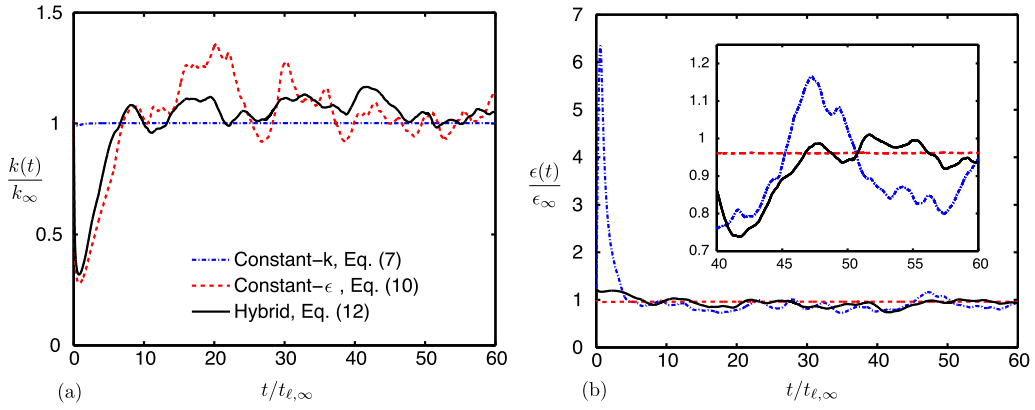

FIG. 2. DNS comparisons of the time development of (a) turbulent kinetic energy and (b) turbulent dissipation for the three proposed forcing methods (7), (10), and (12), with $G = H = 67$ (see legend in panel (a)).

hand, order-unity values of G and H lead to longer transient periods and offset errors in k and ϵ, respectively. Offset errors in k occur when the proximity of k to k_∞ is sufficiently small such that $(k - k_\infty)/k_\infty \sim \Delta\epsilon/(G\epsilon_\infty)$, where $\Delta\epsilon$ is the numerical error emerging from the mismatch between the discretization of the turbulent dissipation in Eqs. (4) and (7), the former being fixed by the energy-preserving numerical scheme used to solve the momentum equation (1). When both discretizations are the same, the offset error vanishes. For illustration, different discretizations were used in Figs. 3(a) and 3(b), which led to $\Delta\epsilon/\epsilon_\infty \sim 3\%$ for $G = 0.67$, consistent with the 5% offset error in k observed in Fig. 3(a). As a result, the upper bound of the offset error decreases rapidly

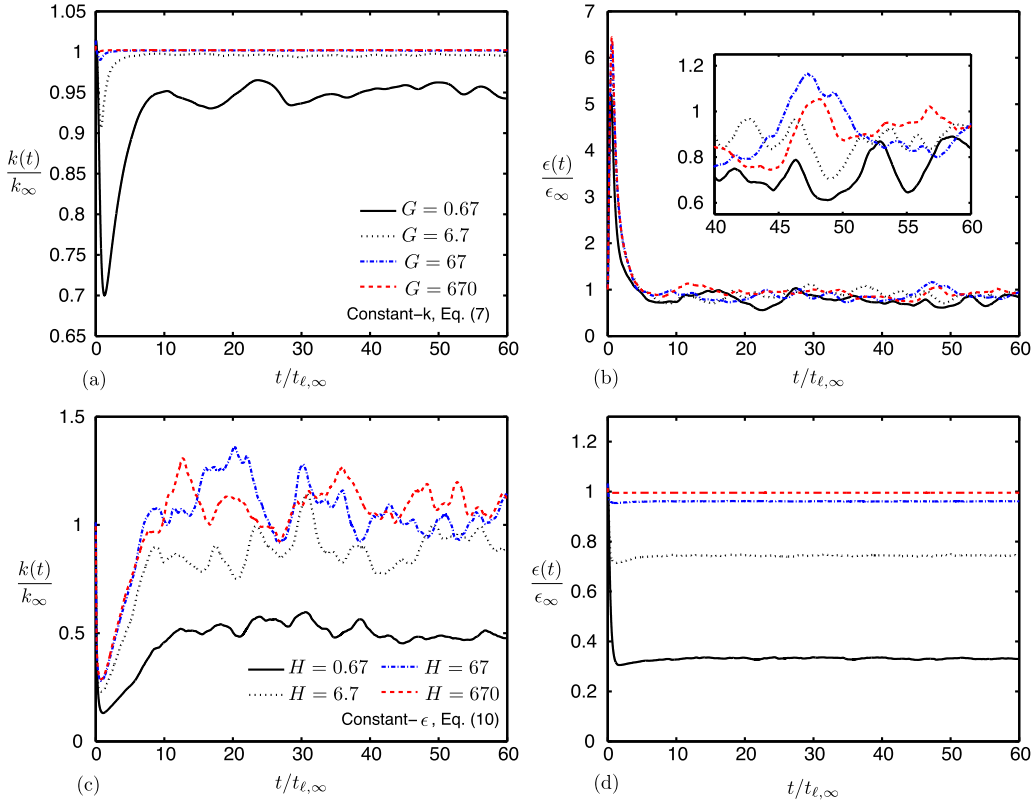

FIG. 3. DNS effects of varying the proportional gains G in Eq. (7) (upper panels) and H in Eq. (10) (lower panels). The figure shows the resulting time dependence of (a,c) turbulent kinetic energy and (b,d) turbulent dissipation. Line types are defined in panels (a) and (c).

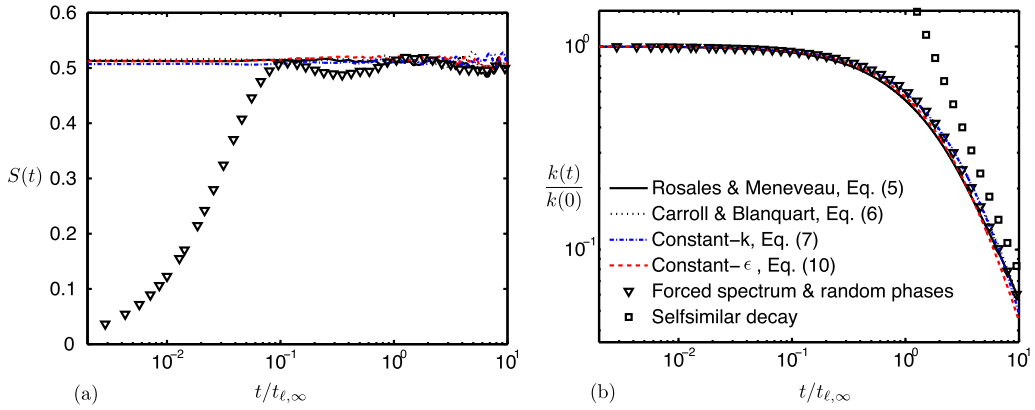

FIG. 4. DNS comparisons of decaying turbulence after deactivation of the corresponding forcing method for (a) velocity-derivative skewness and (b) turbulent kinetic energy, with time origin being reset to the instant of deactivation.

with increasing G, as shown in Fig. 3(a). The offset error in ϵ shown in Fig. 3(d) is caused by an equivalent effect in Eq. (10) that arises from differences between the discretizations of w and the first two terms on the right-hand side of Eq. (9). In summary, large values of G and H are preferred over order-unity values for faster convergence and for general non-energy-preserving schemes, provided that the corresponding time step in the numerical integrations is sufficiently small to resolve the controller's time constants $t_{\ell,\infty}/G$ or $t_{\ell,\infty}/H$, both of which shall be chosen to be shorter than the Kolmogorov timescale $t_{k,\infty}$ in order to avoid interference with energy-containing time scales of the turbulence. It is worth mentioning that a similar impact of numerical errors was observed in Ref. 8 in the context of forcing for scalars.

C. Initialization of decaying turbulence with forced flows

The analysis described above deals primarily with forced turbulent flows. A physically realizable scenario for studying Navier-Stokes turbulence is that of decaying turbulent flows, such as those generated in air flowing through grids in wind tunnels. The purpose of this section is to investigate whether initial conditions obtained from the application of the forcing methods proposed here introduce artificial transient behavior in the decaying dynamics of turbulence. The DNS flow fields described in Section III were left to decay by deactivating the forcing at $t = 43t_\ell$. Comparisons were made among those and an additional decaying field synthetically obtained by reconstructing an initial velocity field from the energy spectrum resulting from a calculation with the forcing coefficient Eq. (7) supplemented with random phases and a divergence-free condition.

The corresponding results are shown in Fig. 4 along with Kolmogorov's selfsimilar decay rate $t^{-10/7}$ (see Ref. 9). Although the five flows require approximately one integral time of decorrelation for adjustment to self-similar decaying turbulence, the velocity-derivative skewness of the initially synthetic flow reaches its expected value after a transient of order $t \sim 0.1t_{\ell,\infty}$. Figure 4(a) shows that the initially forced flows, on the other hand, provide steadier velocity-derivative skewness throughout the decay implying that the energy-cascade process remains in equilibrium. After the transient period, the turbulent flows initially forced with the coefficients (5) and (10) display energy deficits caused by the initially faster decays, as shown in Fig. 4(b).

IV. LES RESULTS AND COMPARISONS

The LES results shown below make use of the dynamic Smagorinsky subgrid-scale model[12,13] subject to a box-type test filter. A grid with 32^3 elements is utilized, which is equivalent to a resolution $\kappa_{max}\ell_{k,\infty} = 0.13$. The corresponding initial conditions are generated from the initial model spectrum (3) as described in Section I, subject to the same input parameters outlined in Section III except κ_0, which is varied below in order to illustrate the effects of initial conditions in coarse calculations.

A. LES formulation of constant-energetics control-based forcing coefficients

Before describing the results, it is worth emphasizing that Eq. (4) ceases to be useful in LES since part of the exact turbulent kinetic energy is unresolved. The relevant quantity in this part of the study is the spatially averaged resolved kinetic energy, $k_r(t) = \langle \overline{u}_i \overline{u}_i \rangle/2$, where the overbar operator denotes resolved velocities. In particular, multiplication of the filtered version of the momentum conservation equation (1) by the resolved velocity, along with spatial averaging of the resulting kinetic-energy transport equation, leads to

$$\frac{dk_r}{dt} = -\epsilon_r - \epsilon_{\mathrm{SGS}} + 2Ak_r. \tag{13}$$

In this formulation, $\epsilon_r = \langle \nu(\partial \overline{u}_i/\partial x_j)(\partial \overline{u}_i/\partial x_j) \rangle$ is the resolved molecular dissipation and $\epsilon_{\mathrm{SGS}} = \langle \nu_{\mathrm{SGS}}(\partial \overline{u}_i/\partial x_j)(\partial \overline{u}_i/\partial x_j) \rangle$ is the subgrid-scale dissipation, with ν_{SGS} being an eddy viscosity computed as in Ref. 13. At sufficiently high Reynolds numbers, the ratio $\epsilon_r/\epsilon_{\mathrm{SGS}} \sim \nu/\nu_{\mathrm{SGS}}$ is small and scales as $(\kappa_{max}\ell_{k,\infty})^{4/3} \ll 1$. In the present computations at moderately large Reynolds numbers, however, both quantities are added to yield an overall dissipation $\epsilon_T = \epsilon_r + \epsilon_{\mathrm{SGS}}$ in defining the forcing coefficient, although this extension is not required for the performance of the methods.

In the following, references are made to LES results obtained by using the previous forcing coefficients (5) and (6). The LES versions of these coefficients employ the values k_∞ and ϵ_∞ corresponding to the target values of k_r and ϵ_T, respectively, with $k_r(t)$ being also used in (6) instead of $k(t)$. Similarly, the LES version of the proposed constant-k forcing coefficient (7) becomes

$$A(t) = \frac{\epsilon_T - G[k_r(t) - k_\infty]/t_{\ell,\infty}}{2k_r(t)}, \tag{14}$$

which transforms Eq. (13) into a form similar to Eq. (8) in terms of the resolved kinetic energy $k_r(t)$.

Constant-ϵ forcing in LES is achieved by applying a proportional controller to the conservation equation

$$\begin{aligned}
\frac{d\epsilon_T}{dt} &= -2\left\langle (\nu + \nu_{\mathrm{SGS}}) \frac{\partial \overline{u}_i}{\partial x_k} \frac{\partial \overline{u}_j}{\partial x_k} \frac{\partial \overline{u}_i}{\partial x_j} \right\rangle \\
&+ 2\left\langle (\nu + \nu_{\mathrm{SGS}}) \frac{\partial \overline{u}_i}{\partial x_k} \frac{\partial}{\partial x_k} \left\{ \frac{\partial}{\partial x_j} \left[(\nu + \nu_{\mathrm{SGS}}) \left(\frac{\partial \overline{u}_i}{\partial x_j} + \frac{\partial \overline{u}_j}{\partial x_i} \right) \right] \right\} \right\rangle \\
&- \left\langle \nu_{\mathrm{SGS}} \frac{\partial}{\partial x_j} \left(u_j \frac{\partial \overline{u}_i}{\partial x_k} \frac{\partial \overline{u}_i}{\partial x_k} \right) \right\rangle + \left\langle \frac{\partial \nu_{\mathrm{SGS}}}{\partial t} \frac{\partial \overline{u}_i}{\partial x_k} \frac{\partial \overline{u}_i}{\partial x_k} \right\rangle - 2\left\langle \nu_{\mathrm{SGS}} \frac{\partial}{\partial x_i} \left[\frac{\partial \overline{u}_i}{\partial x_k} \frac{\partial}{\partial x_k} \left(\frac{\overline{p}}{\rho} \right) \right] \right\rangle + 2A\epsilon_T,
\end{aligned} \tag{15}$$

which is obtained by differentiating the LES version of (1) with respect to x_k, multiplying the resulting equation by $2(\nu + \nu_{\mathrm{SGS}})\partial \overline{u}_i/\partial x_k$, regrouping terms, and spatially averaging over the periodic domain. Note that Eq. (15) is contingent on the eddy-viscosity assumption and becomes equal to Eq. (9) in the limit $\nu_{\mathrm{SGS}} \to 0$. Based on Eq. (15), the LES version of the constant-ϵ forcing coefficient (10) becomes

$$A(t) = -\frac{f(t) + H[\epsilon_T(t) - \epsilon_\infty]/t_{\ell,\infty}}{2\epsilon_T(t)}, \tag{16}$$

where $f(t)$ is the sum of the first four terms on the right hand side of (15).

A hybrid forcing coefficient can be easily formulated for LES based on (14) and (16) using the same least-squares minimization procedure as in Section II C to maintain approximately the constant-k and constant-ϵ conditions. The resulting expression,

$$\begin{aligned}
A(t) = &\frac{4k_r^2(t)}{4k_r^2(t) + 9t_{\ell,\infty}^2\epsilon_T^2(t)} \left(\frac{\epsilon_T - G[k_r(t) - k_\infty]/t_{\ell,\infty}}{2k_r(t)} \right) \\
&- \frac{9t_{\ell,\infty}^2\epsilon_r^2(t)}{4k_r^2(t) + 9t_{\ell,\infty}^2\epsilon_T^2(t)} \left(\frac{f(t) + H[\epsilon_T(t) - \epsilon_\infty]/t_{\ell,\infty}}{2\epsilon_T(t)} \right),
\end{aligned} \tag{17}$$

yields intermediate results with respect to (14) and (16).

B. Convergence in physical and spectral spaces

Comparisons are made in Fig. 5 between LES, subject to the initial model spectrum (3) with $\kappa_0 = 6.25$, using forcing coefficients (5), (6), (14), and (16). The results show that the constant-k coefficient (14) leads to faster convergence and steadier statistics both in spectral and physical spaces, with the three methods (5), (6), and (14) tending to under-predict the dissipation with respect to its target statistically stationary value, as seen in Fig. 5(b). The constant-ϵ coefficient (16), on the other hand, tends to over-predict the resolved kinetic energy, as shown in Fig. 5(a), which leads to spectra lying outside of the envelopes predicted by using (5) (e.g., see Fig. 5(c)).

In terms of relative spectral variations in time, Fig. 5(d) shows that the constant-k method yields the most satisfactory results, with method (5) yielding the largest fluctuations. In summary, the conclusions from the LES comparisons are analogous to those drawn from the DNS results in Section III.

C. Forcing-driven restoration of the direct energy cascade

Unlike DNS, for which it is known that the choice of the initial condition impacts weakly the forced steady-state solution, the results presented here suggest that the choice of the initial condition can have considerable influences on forced LES. For instance, in this study, it is observed that the constant-k method (14) displays more robustness than the other methods in LES simulations under initial conditions that favor the occurrence of subgrid-scale backscatter. In particular, LES simulations were carried out for $\kappa_0 = 12.5$ in (3), which displaced the maximum of the initial spectrum toward

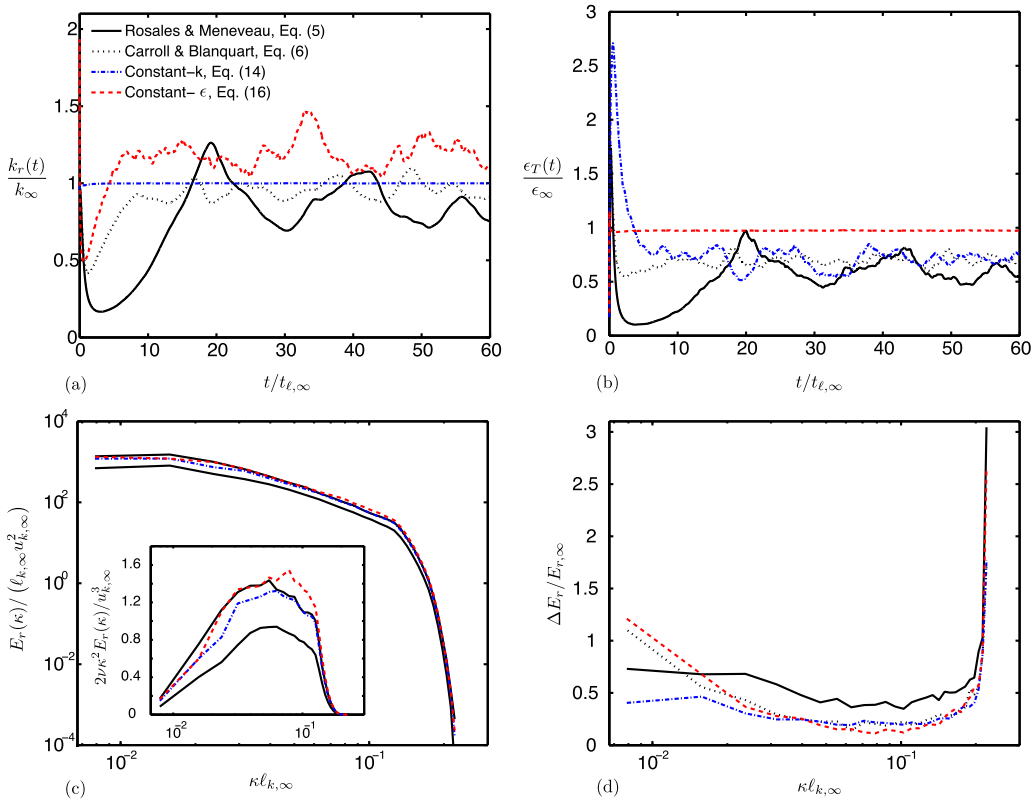

FIG. 5. LES comparisons of the proposed forcing methods, with $G = H = 67$ and $\kappa_0 = 6.25$, against the forcing methods in Refs. 4 and 6 (see legend in panel (a) for line types). The upper panels include the time dependence of (a) resolved kinetic energy and (b) overall dissipation. The lower panels show the instantaneous spectra for (c) resolved kinetic energy and resolved viscous dissipation (inset) at $t = 5.7t_{\ell,\infty}$ along with the envelope represented by the maximum and minimum values resulting from employing (5) during long periods of time $t = 43t_{\ell,\infty} - 72t_{\ell,\infty}$ (solid lines). Panel (d) shows the normalized amplitude of the envelopes produced by the maximum and minimum values of the kinetic-energy spectra observed during the time interval $t = 43t_{\ell,\infty} - 72t_{\ell,\infty}$ for all four methods.

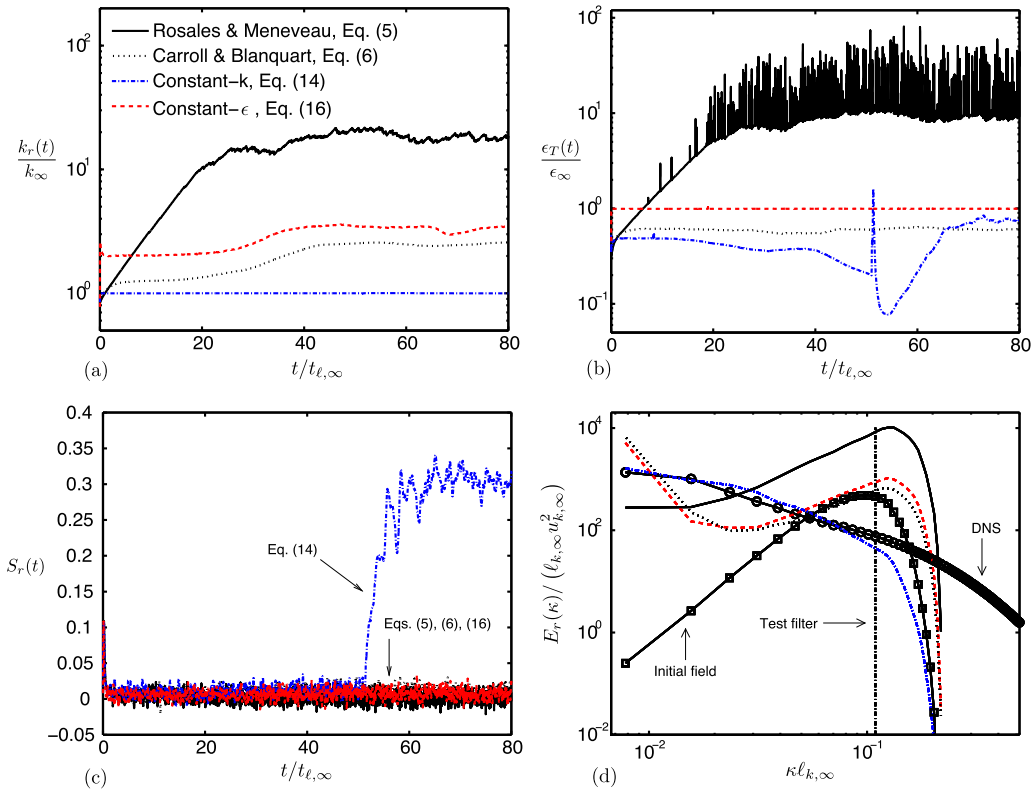

FIG. 6. LES comparisons of the proposed forcing methods, with $G = H = 67$ and subject to the initial spectrum (3) with $\kappa_0 = 12.5$, against previous ones, including the time dependence of (a) resolved kinetic energy, (b) overall dissipation, (c) skewness of the resolved velocity derivative (see legend in panel (a)), and (d) instantaneous resolved kinetic-energy spectra at $t = 70t_{\ell,\infty}$.

higher wavenumbers in contrast to the results presented in Fig. 5, which were obtained using a smaller κ_0. With the initial condition corresponding to $\kappa_0 = 12.5$, the resulting dynamics, portrayed in Fig. 6, lead initially to net subgrid-scale backscatter manifested in the dynamic model by negative eddy viscosities (which are clipped in the computations). The results reveal that the forcing coefficients (5) and (6), along with the constant-ϵ one (16), offer no useful alternative to the constant-k coefficient (14) in restoring the direct energy cascade. Specifically, Figs. 6(a) and 6(b) show that the forcing coefficients (5), (6), and (16) lead to unphysical dynamics, and the resulting skewness of the resolved velocity derivative, defined as $S_r = -\langle(\partial\overline{u}_1/\partial x_1)^3\rangle/[\langle(\partial\overline{u}_1/\partial x_1)^2\rangle]^{3/2}$, does not correspond to that of a turbulent flow,[14] as shown in Fig. 6(c). The vortical fields corresponding to the resulting non-turbulent flows are shown in Fig. 7(a), which are primarily characterized by large-scale round blobs remnants from the initial field that do not produce enough dissipation. Similarly, the corresponding kinetic-energy spectra, obtained using either (5), (6), or (16) and evaluated at $t = 70t_{\ell,\infty}$, contain energy maxima at high wavenumbers that suggest insufficient dissipation rates and are contrary to the Kolmogorov inertial-subrange scaling, as observed in Fig. 6(d). The constant-ϵ method (16) is incapable of establishing the correct ϵ_{SGS} despite the action of the controller, in that the resolved molecular dissipation ϵ_r attains values close to the target overall dissipation ϵ_∞, whereas the subgrid-scale dissipation remains $\epsilon_{\mathrm{SGS}} = 0$ during the simulation because of clipping. This prevents the development of turbulence. Unclipped simulations were found to be unstable and provided no meaningful results.

On the other hand, the LES subjected to the proposed constant-k forcing coefficient (14) attains physical results for $t \gtrsim 50t_{\ell,\infty}$ that resemble forced LES turbulence, as shown in Figs. 6(c) and 6(d). During the period prior to the transition, $t \lesssim 50t_{\ell,\infty}$, an energy pile-up is observed in the spectrum similar to those obtained by using the forcing coefficients (5), (6), and (16), with the vortical structures in the flow resembling those shown in Fig. 7(a). A transition to turbulence occurs at $t \sim 50t_{\ell,\infty}$ that is related to the intermittency in ϵ_{SGS} and the sensitivity of the forcing coefficient (14) to

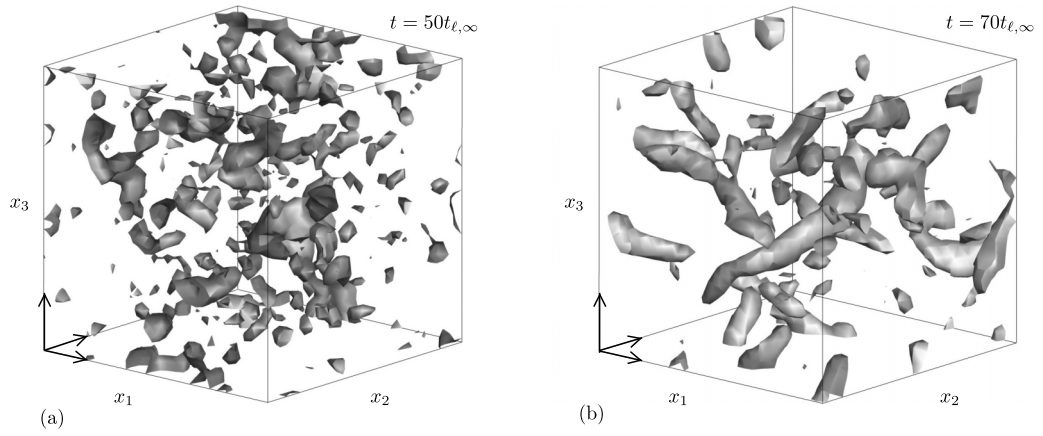

FIG. 7. LES isosurfaces of the square root of the local enstrophy ω obtained using the proposed constant-k forcing coefficient (14) with $G = 67$, (a) before transition ($\omega\ell_\infty/u_{\ell,\infty} = 6.25$) and (b) after transition to forced LES turbulence ($\omega\ell_\infty/u_{\ell,\infty} = 11.3$). The initial spectrum (3) is imposed at the beginning of the simulations with $\kappa_0 = 12.5$.

ϵ_{SGS}. Specifically, ϵ_{SGS} reaches positive values at the transition time that overwhelm the viscous dissipation and persist thereon aided by the fact that the constant-k coefficient (14) is proportional to ϵ_{SGS}. After the transition point $t \sim 50t_{\ell,\infty}$, the pile-up of energy disappears, indicating establishment of a net forward cascade of energy. The resulting LES flow field displays vortical structures that resemble physical worm-like patterns enabled by the three-dimensional vortex-stretching mechanism,[15] as shown in Fig. 7(b). The corresponding velocity-derivative skewness S_r attains values similar to the reference ones,[14] as observed in Fig. 6(c). Although the corresponding transient period is about ten times longer than in DNS, the flow forced with the proposed constant-k coefficient (14) reaches a state in which the spectrum and time series of resolved kinetic energy have minimal oscillations, while 10%-20% fluctuation amplitudes are observed in skewness and dissipation.

Additional LES computations (not shown here for brevity) were performed using a converged turbulent flow field forced with the constant-k coefficient as initial condition for separate simulations forced with coefficients (5), (6), and (16), which, as shown in Fig. 6, do not provide physical solutions. In the results, the turbulent flow remained converged, in that k and ϵ were close to the target stationary values k_∞ and ϵ_∞, the value of the skewness of the resolved velocity derivative was on the upper branch of Fig. 6(c), and the turbulent kinetic-energy spectrum was similar to that shown in dashed-dotted lines in Fig. 6(d). These considerations highlight the effect of initial conditions in forced LES, in that the forcing methods (5), (6), and (16), which failed to restore the direct kinetic-energy cascade, sustained a converged LES turbulent flow when provided as initial condition to the simulations.

V. INFLUENCES OF FORCING APPROACHES ON DILUTE PARTICLE-LADEN HOMOGENEOUS-ISOTROPIC TURBULENCE

Linear forcing is widely used in numerical simulations of particle-laden homogeneous-isotropic turbulent flows, the reason being that forcing turbulence enables collection and analysis of stationary disperse-phase statistics of, for instance, relative dispersion, preferential concentration, and particle acceleration. However, it is known that linear forcing interferes with the transfer of kinetic energy from particles to the fluid in two-way coupled flows.[16] As a result, the utilization of linearly forced turbulence is typically precluded to one-way coupled flows, this being the case addressed here in which the mass-loading ratio (defined below) remains small and the corresponding effects of particles on the carrier phase become negligible. In this section, a brief analysis is reported that treats the influences of forcing, along with the associated fluctuations in statistics observed in Section III, on the disperse-phase statistics. In particular, the physical-space forcing treated above can lead to fluctuations in quantities that define turbulence scales. Such scales are, in turn, fundamental for the dynamics of particles in turbulent flows.[17]

A. Formulation of the disperse phase

The computations outlined in this section employ the same numerical code and DNS input parameters described in Section III. The disperse-phase formulation is based on a Lagrangian description for small particles, including the trajectory equation

$$\frac{dx_{p,i}}{dt} = u_{p,i} \tag{18}$$

and the equation of motion

$$\frac{4}{3}\pi\rho_p a^3 \frac{du_{p,i}}{dt} = 6\pi\rho\nu a(u_i - u_{p,i}), \tag{19}$$

where $x_{p,i}$ and $u_{p,i}$ denote, respectively, the position and velocity of the particles. Additionally, ρ_p and a refer to the particle density and radius, respectively. Small particle Reynolds numbers, $\mathrm{Re}_p = [(u_{p,i} - u_i)(u_{p,i} - u_i)]^{1/2}a/\nu \ll 1$, have been assumed in writing (19). In particular, Eq. (19) describes a characteristic relaxation of the particle velocity to the local velocity of the fluid in an acceleration time scale of order $t_a \sim (2/9)(\rho_p/\rho)(a^2/\nu)$, with the Stokes number $\mathrm{St}_k = t_a/t_{k,\infty} =$ 0.1, 1, and 30 measuring the ratio of t_a to the steady Kolmogorov turnover time $t_{k,\infty}$. Additionally, a small mass-loading ratio $\alpha = (4/3)(\rho_p/\rho)\pi N_p(a/L)^3 = 3 \times 10^{-6}$ is employed, with $N_p = 96\,000$ particles being seeded initially in the carrier phase. At the beginning of the computations, the particles are positioned in space according to a uniform random distribution under kinematic equilibrium with the carrier phase. The resulting transient time measured from the initialization of the spatial distribution of particles is of order t_a and therefore has negligible impact on the results presented here. In the simulations, Eqs. (1) and (2), along with the Lagrangian particle equations (18) and (19), are integrated subjected to an initial velocity field of homogeneous-isotropic turbulence extracted at $t = 43t_{\ell,\infty}$ from the DNS performed in Section III for each one of the four forcing approaches (5), (6), (7), and (10). A mid-plane cross section of the simulations is presented in Fig. 8(a) that shows the contours of the square root of the local enstrophy.

B. Numerical results and comparisons

For $\mathrm{St}_k = 0.1$, the flow regime resembles one in which the particles are mostly tracers, in that their motion becomes sensitive to the large-scale kinetic energy of the carrier phase as well as to the associated velocity fluctuations arising from the forcing approach. This is illustrated in the top panel in Fig. 8(b), which shows the time development of the particle kinetic energy $k_p = \langle u_{p,i}u_{p,i}\rangle_{N_p}/2$, where the operator "$\langle f\rangle_{N_p}$" denotes the average of the Lagrangian variable f over all the particles. It is observed that the proposed constant-k forcing coefficient (7) leads to minimal fluctuations in the particle kinetic energy in accord with the carrier-phase dynamics observed in Fig. 1(a), thereby enabling stationarity in the statistics for the disperse-phase energetics. On the contrary, utilization of the forcing coefficients (5), (6), and (10) causes considerable oscillations in the particle kinetic energy of order 20%-40%. Increasing the Stokes number, however, diminishes the advantage of using the constant-k forcing (7). For instance, for $\mathrm{St}_k = 1$, the particles are tracers for the large-scale eddies but slip on the Kolmogorov ones, and for $\mathrm{St}_k = 30$, the particles become ballistic with respect to most eddies except for the large ones with which they interact since the corresponding integral-scale Stokes number $\mathrm{St}_\ell = (\ell_{k,\infty}/\ell_\infty)^{2/3}\mathrm{St}_k$ becomes an order-unity parameter. As a result, the kinetic energy of the particles increasingly deviates from that of the fluid for increasing Stokes numbers, which leads to oscillatory behavior in k_p that cannot be suppressed by any of the forcing methods, as shown in the lower panel in Fig. 8(b).

Statistics of the particle acceleration $a_p = \langle[(du_{p,i}/dt)(du_{p,i}/dt)]^{1/2}\rangle_{N_p}$ normalized with the target Kolmogorov acceleration $a_{k,\infty} = u_{k,\infty}/t_{k,\infty}$ are shown in Fig. 8(c). While the constant-k forcing renders stationary statistics for the kinetic energy of sufficiently light particles, the constant-ϵ forcing yields steadier probability density functions (PDFs) of the particle acceleration insofar as the Kolmogorov-based Stokes number St_k is not too large, as implied by the corresponding PDF envelopes. In particular, for moderate values of St_k, the characteristic acceleration of the particles is comparable to the Kolmogorov acceleration, since the relative motion with respect to the large

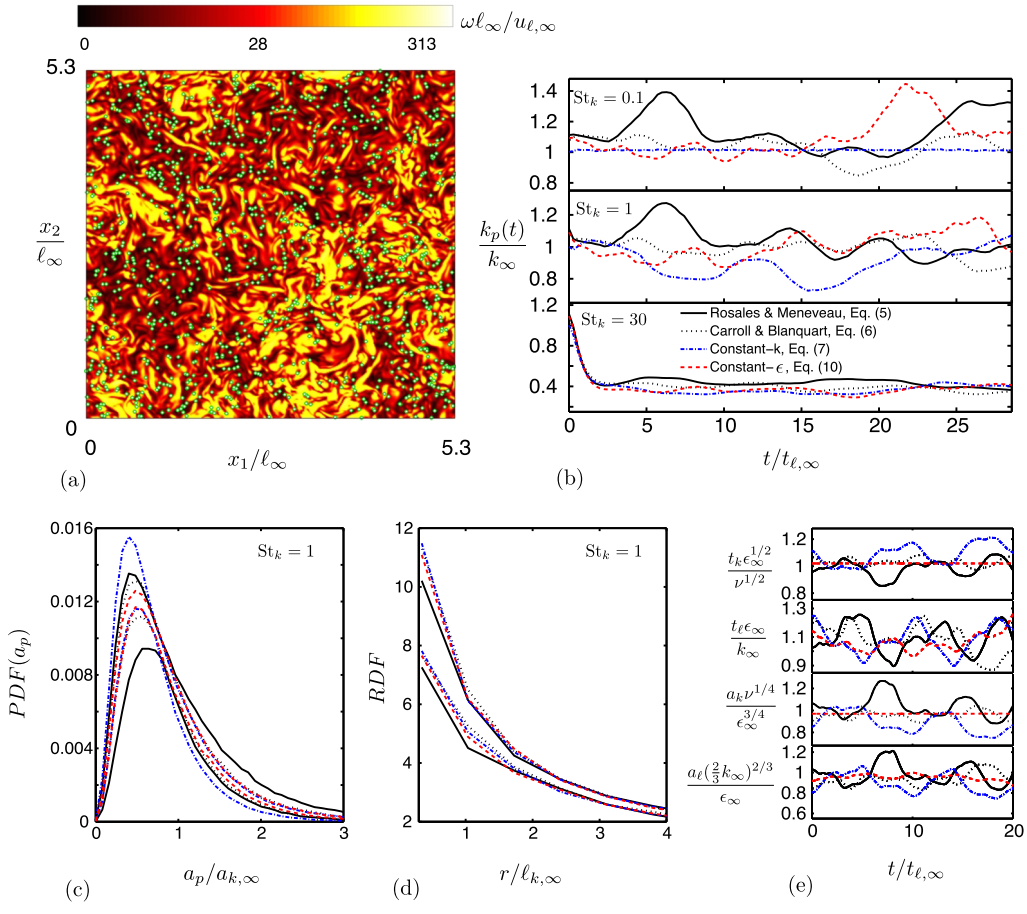

FIG. 8. (a) Mid-plane cross section of the isosurfaces of the square root of the local enstrophy (solid contours) along with the spatial distribution of particles (green dots) contained in a x_3 slice of thickness $0.06\ell_\infty$. (b) Time series of the average particle kinetic energy with time origin being reset to the instant of particle deployment. (c) Particle acceleration PDF and (d) radial distribution function long-time envelopes of the four different methods produced by the maximum and minimum values of the corresponding quantity observed during the time interval $t = 5t_{\ell,\infty} - 25t_{\ell,\infty}$. (e) Time series of integral and Kolmogorov characteristic acceleration and time scales. The values $G = H = 67$ are used here for evaluating (7) and (10).

scales is negligible. The reason for the steadier behavior of the PDF of a_p therefore lies in the constancy of the Kolmogorov scales resulting from the constant dissipation obtained by using the forcing approach (10). This is shown in Fig. 8(e), which additionally reveals that the integral scales, including the integral acceleration a_ℓ, fluctuate in time independently of the forcing approach employed. As a result, strong fluctuations are obtained in all metrics when the characteristic dynamics of the particles are influenced by scales above the Kolmogorov range.

The choice of forcing does not have any noticeable influence on the time dynamics of the preferential concentration. The preferential-concentration phenomenon, which is known to become most intense near $\mathrm{St}_k = 1$, is quantified by the radial distribution function (RDF) shown in Fig. 8(d), which refers to the likelihood of any pair of particles being separated by a given distance (see, for instance, Section 1 in Ref. 18 for a mathematical definition of the RDF). Convergence studies were carried out increasing the number of particles that ruled out statistical variabilities caused by under-sampling of the particle ensemble. No clear variation patterns are observed for the fluctuations in the RDF when the different forcing methods are employed. In particular, the constancy of the Kolmogorov scales achieved with the constant-ϵ forcing method does not appear to be relevant for decreasing the fluctuations in the RDF. In practice, this results in large time windows (larger than $20t_{\ell,\infty}$) required for the collection of converged preferential-concentration statistics whichever one of the four forcing methods is employed.

The different forcing approaches lead to small variations of order 10%–20% in the temporal averages of the statistics analyzed here, as easily inferred from Fig. 8. There is no fundamental cause by which the temporal averages should be different after long times, since the turbulence state targeted by the different forcing methods is the same. In practice, however, exceedingly long time windows would be required in the carrier phase to obtain matched time-averaged statistics of the disperse phase. This can be understood, for instance, by examining Figs. 1(a) and 1(b) or 8(e) and noticing that convergence of time-averaged statistics in the carrier phase is hardly achieved after several integral times.

VI. CONCLUDING REMARKS

Constant-energetics, control-based linear forcing approaches for incompressible homogeneous isotropic turbulence have been presented in Eqs. (7) and (10) for DNS and in Eqs. (14) and (16) for LES. The methods consist of proportional controllers embedded in the forcing coefficients. In particular, the forcing coefficients (7) and (14) submit the kinetic energy to its statistically steady target value after short transients of the same order as the integral time of the turbulence divided by a large constant gain. The forcing coefficients (10) and (16) provide constant dissipation close to its statistically steady value in a similar way. Approximate combined forcing at constant energy and constant dissipation is achieved through the coefficients (12) in DNS and (17) in LES, which make use of least-squares minimization. Compared to the approaches in Refs. 4 and 6 and starting from the same initial flow field, the methods proposed in this investigation provide forced turbulent flows in shorter times, resulting in steadier statistics of kinetic energy and dissipation in both physical and spectral spaces. Additionally, the proposed constant kinetic-energy forcing method (14) behaves more robustly under an initial condition that imposes a reverse cascade in the coarse LES computations analyzed here, in that it operates to establish a direct energy cascade yielding turbulent flows, while the other approaches provide unphysical fields. When applied to DNS of dilute particle-laden homogeneous-isotropic turbulent flows, the proposed constant kinetic-energy forcing approach (7) leads to stationary statistics for the disperse-phase kinetic energy at small Stokes numbers, while the alternative methods yield large-amplitude oscillations. Similarly, the constant-dissipation forcing method (10) provides steadier statistics for the acceleration of light particles. However, all the forcing methods yield similar fluctuations in preferential-concentration metrics.

In principle, there is no obstacle for employing the proposed constant-k coefficient (7) for band-limited forcing in spectral space, provided that it is reformulated as

$$A(\kappa,t) = \begin{cases} \dfrac{\epsilon(t) - G[k_f(t) - k_\infty]/t_\ell}{2k_f(t)}, & \text{if } 0 < \kappa < \kappa_f \\ 0, & \text{otherwise} \end{cases}, \tag{20}$$

where k_∞ is the target value of k_f, with $k_f = \int_0^{\kappa_f} E(\kappa)d\kappa$ being the kinetic energy of the wavenumber band $0 < \kappa < \kappa_f$. In this formulation, κ_f is a cutoff wavenumber in the inertial subrange that bounds the forced spectral band, with $\kappa_f \to \infty$ representing the case equivalent to physical-space linear forcing described in Secs. I–V. The resulting conservation equation for the turbulent kinetic energy $k_f(t)$ has a form similar to Eq. (4).

ACKNOWLEDGMENTS

The authors acknowledge useful discussions with Ohi Dibua on this topic. This investigation was funded by the Advanced Simulation and Computing (ASC) program of the US Department of Energy's National Nuclear Security Administration via the PSAAP-II Center at Stanford.

[1] T. S. Lundgren, "Linearly forced isotropic turbulence," in *Annual Research Briefs* (Center for Turbulence Research, 2003), pp. 461-473.

[2] T. Passot and A. Pouquet, "Numerical simulation of compressible homogeneous flows in the turbulent regime," J. Fluid Mech. **181**, 441-466 (1987).

[3] M. R. Overholt and S. B. Pope, "A deterministic forcing scheme for direct numerical simulations of turbulence," Comput. Fluids **27**, 11-28 (1998).
[4] C. Rosales and C. Meneveau, "Linear forcing in numerical simulations of isotropic turbulence: Physical space implementations and convergence properties," Phys. Fluids **17**, 095106 (2005).
[5] B. de Laage de Meux, B. Audebert, R. Manceau, and R. Perrin, "Anisotropic linear forcing for synthetic turbulence generation in large eddy simulation and hybrid RANS/LES modeling," Phys. Fluids **27**, 035115 (2015).
[6] P. L. Carroll and G. Blanquart, "A proposed modification to Lundgren's physical space velocity forcing method for isotropic turbulence," Phys. Fluids **25**, 105114 (2013).
[7] L. Machiels, "Predictability of small-scale motion in isotropic fluid turbulence," Phys. Rev. Lett. **79**, 3411-3414 (1997).
[8] P. L. Carroll, S. Verma, and G. Blanquart, "A novel forcing technique to simulate turbulent mixing in a decaying scalar field," Phys. Fluids **25**, 095102 (2013).
[9] A. N. Kolmogorov, "On degeneration of isotropic turbulence in an incompressible viscous liquid," C. R. Akad. Sci. SSSR (Dokl.) **31**, 538-540 (1941).
[10] H. Pouransari, H. Kolla, J. Chen, and A. Mani, "Spectral analysis of energy transfer in variable density, radiatively heated particle-laden flows," in *Proceedings of the Summer Program 2014* (Center for Turbulence Research, Stanford University, 2014), pp. 27-36.
[11] H. Pouransari, M. Mortazavi, and A. Mani, "Parallel variable-density particle-laden turbulence simulation," in *Annual Research Briefs 2015* (Center for Turbulence Research, Stanford University, 2015), pp. 43-54.
[12] M. Germano, U. Piomelli, P. Moin, and W. H. Cabot, "A dynamic subgrid-scale eddy viscosity model," Phys. Fluids **3**, 1760-1765 (1991).
[13] D. K. Lilly, "A proposed modification of the Germano subgrid scale closure method," Phys. Fluids **4**, 633-634 (1992).
[14] S. Tavoularis, J. C. Bennett, and S. Corrsin, "Velocity derivative skewness in small Reynolds number, nearly isotropic turbulence," J. Fluid Mech. **88**, 63-69 (1978).
[15] J. Jiménez, A. A. Wray, P. G. Saffman, and R. S. Rogallo, "The structure of intense vorticity in isotropic turbulence," J. Fluid Mech. **255**, 65–90 (1993).
[16] G. Mallouppas, W. K. George, and B. G. M. van Wachem, "New forcing scheme to sustain particle-laden homogeneous and isotropic turbulence," Phys. Fluids **25**, 083304 (2013).
[17] J. Urzay, M. Bassenne, G. I. Park, and P. Moin, "Characteristic regimes of subgrid-scale coupling in LES of particle-laden turbulent flows," in *Annual Research Briefs* (Center for Turbulence Research, Stanford University, 2014), pp. 3–13.
[18] B. Ray and L. R. Collins, "Preferential concentration and relative velocity statistics of inertial particles in Navier-Stokes turbulence with and without filtering," J. Fluid Mech. **680**, 488–510 (2011).